論文 / 著書情報
Article / Book Information

Title	Adhesion strength of paraffin droplet impacted and solidified on metal substrate
Authors	Chao Kang, Motoki Sakaguchi, Akito Saito, Hirotsugu Inoue
Citation	Results in Physics, Vol. 34, , p. 105310
Pub. date	2022, 2
DOI	https://doi.org/10.1016/j.rinp.2022.105310
Creative Commons	Information is in the article.

Results in Physics 34 (2022) 105310

Contents lists available at ScienceDirect

Results in Physics

journal homepage: www.elsevier.com/locate/rinp

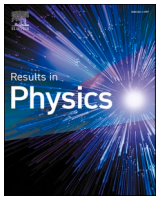

Adhesion strength of paraffin droplet impacted and solidified on metal substrate

Chao Kang, Motoki Sakaguchi *, Akito Saito, Hirotsugu Inoue

Department of Mechanical Engineering, Tokyo Institute of Technology, O-okayama, 2-12-1, Meguro-ku, Tokyo 152-8552 Japan

ARTICLE INFO

Keywords:
Debonding
Adhesion strength
Single splat
Scraping test
Thermal spraying

ABSTRACT

Debonding of solidified splats is a crucial issue for thermal sprayed coatings, which greatly influences the performance and lifetime of industrial components. The purpose of this study is to provide an in-depth understanding of the effects of impact parameters as well as residual stress on the debonding behaviors, and the related adhesion strength and driving forces of single splats. In this study, debonding behaviors of molten paraffin droplets which were impacted and solidified on stainless steel substrates, were observed considering the effects of substrate pre-set temperature, drop height (impact velocity), and droplet temperature. It was found that the debonding is prone to take place at lower substrate pre-set temperatures, lower drop heights, and lower droplet temperatures. A scraping method was then employed to measure the adhesion strength of splats formed under various conditions. The results showed good accordance with debonding behaviors in the drop impact test. The scraping tests also indicated that the residual tensile stress in splats reduces the scraping forces and prevents the complete removal of splats during the scraping processes. Peeling stress and shear stress along the splat-substrate interface, which are driving forces for debonding, were calculated using coupled thermomechanical finite element analyses. The calculated driving forces were larger for lower drop heights and lower droplet temperatures under which the debonding was more easily to occur. The results of numerical simulations coupled with scraping tests provide reasonable explanations for observed debonding behaviors of single splats. This study provides a comprehensive understanding of the effects of several droplet impact variables and residual stress on the debonding behaviors, and the related adhesion strength as well as driving forces of single splats.

Introduction

Thermal spraying is one of the most common coating fabrication methods for adding thermal, wear, erosion, or corrosion resistance onto various industrial components such as turbine blades [1], automotive engines [2], and power generation system equipment [3]. During thermal spraying, coating feedstock materials are heated and sprayed onto solid substrates in the form of molten or semi-molten particles to fabricate a dense coating [4]. The coating performance is characterized by many factors, such as density, porosity, thermal conductivity, and adhesion strength. The adhesion between sprayed particles and substrates is mainly attributed to three mechanisms [5]: mechanical interlocking formed due to substrate surface irregularities, physical force from van der Waals interactions, and diffusive-chemical bond caused by diffusion and chemical reactions at the interface. According to Sobolev [6], mechanical interlocking is the major contribution to the interfacial adhesion strength between substrates and thermally sprayed coatings. During thermal spraying, in addition, residual stresses are generated associated with the cooling of splats and substrates [7]. Debonding, referring to the phenomenon that splats peel off from the substrate, occurs when its driving forces exceed the adhesion strength. Here, the driving forces for debonding are the shear stress along the interface and the peeling stress normal to the interface [8]. Adhesion and debonding of splats influence the coating properties and significantly affect the lifetime and performance of the coated components. Therefore, it is of great significance to evaluate and predict the adhesion strength, and to optimize the thermal spraying processes.

Many studies [9 10 11 5] have experimentally investigated the adhesion strength of thermally sprayed coatings, and evaluated the effects of various spraying parameters including substrate surface roughness [9], residual stress [10], heat treatment [11], and particle size [5]. Nevertheless, the reliability of coatings is critically influenced by the characteristics of single splat deposition, and is highly related to the adhesive mechanisms between splats and substrates. Compared with the

* Corresponding author.
E-mail address: sakaguchi.m.ac@m.titech.ac.jp (M. Sakaguchi).

https://doi.org/10.1016/j.rinp.2022.105310
Received 14 November 2021; Received in revised form 23 January 2022; Accepted 3 February 2022
Available online 9 February 2022

extensive studies on the adhesion mechanisms of coatings, only a few publications have been reported to measure the adhesion strength of a single splat due to its extremely small size. In fact, the widely employed pull-off adhesion tests recommended in ASTM D4541-17 [12] and ASTM C633-01 [13] are not appropriate for measuring the adhesion strength of single splats, because it is difficult to efficiently and precisely stick a splat with a loading fixture to ensure the splat can be completely detached from the substrate. Instead, an indentation experiment has been introduced by Balic [14] to evaluate the adhesion strength between alumina splats and steel substrates. A strain release rate was calculated according to interfacial crack propagation to evaluate the strength and mechanisms of the adhesion between single splats and the substrates. Goldbaum [15] measured the adhesion strength of Ti and Ti-6Al-4 V splats which were sprayed onto metal substrates. Shear tests were employed in the measurements where a wedge-shaped stylus was equipped to scratch the splats. The results indicated that the adhesion strength increased with the increase of substrate temperatures and impact velocities. Scratch test has been employed to evaluate the adhesion strength of single splats [16 17 18]. For example, Chen [16] evaluated the adhesion strength of plasma sprayed Fe-based splats on polished metal substrates employing a micro scratch test. The adhesion strength was found to become larger on fully pre-heated substrates due to sufficient spreading of splats and well wettability at the interface. These studies used indentation tests or scratch tests, and investigated the effects of several parameters such as substrate temperatures and impact velocities. However, the effects of impact conditions on splat geometries and the resultant measurements of scratching forces were not investigated. The relationship between the measured adhesion strength and the actual debonding behaviors of splats as well as the debonding driving forces were not fully studied.

Scraping methods have also been applied to evaluate the adhesion strength of coatings. Different from the scratch test, in this method, a cutting blade is equipped to scrape off the coatings from the substrates along the interface [19 20]. Murakawa [19] has proposed a scraping method based on a knife-edge scratch test to evaluate the adhesion strength of diamond coatings. Comparison of the determined adhesion strength with that measured by shearing tests suggested that the scraping method was applicable for evaluating the adhesion strength of hard coatings. Xie [20] measured the adhesion strength of NiP coatings, which were chemically deposited on steel substrates, using a scraping method. The scraping energy, referring to the ratio of measured scraping forces to scraped coating areas, was proposed as a parameter to quantify the interfacial adhesion strength. These studies indicated the scraping tests to be an effective method to evaluate the adhesion strength of sprayed coatings. However, the adhesion strength between single splat and substrate has never been studied by a scraping method yet. Effects of droplet impact parameters and residual stress in splats, which might influence the scraping test results and adhesion strength, need further research.

In the authors' previous studies, molten paraffin droplets were dropped onto stainless steel substrate to investigate the thermal spraying process in an easy and simple manner [8 21 22]. Stress and strain evolutions during the impact, solidification, and cooling processes of droplets were measured to evaluate the effects of various experimental conditions [8 21]. A coupled thermo-mechanical finite element (FE) analysis with a strain hardening creep model was employed to quantify the stress generation process [22]. In this study, similar drop tests are carried out by changing various test variables including substrate pre-set temperature, drop height, and droplet temperature. Debonding behaviors appear at certain conditions due to the thermal stresses originating from the contraction of splats, and the thermal mismatch between splats and substrates. Towards an in-depth understanding of the effects of impact conditions on debonding behaviors of splats, a scraping method is employed to measure the adhesion strength of splats formed under various impact conditions. The effect of residual stress on the adhesion strength is also investigated. The driving forces for debonding are then calculated by using a coupled thermo-mechanical FE analysis.

Experiments

Drop test of paraffin

The drop test was conducted to investigate the effects of impact conditions on debonding behaviors of single splats.

The experimental setup for drop tests, which was improved from the previous setup [8 21] is schematically illustrated in Fig. 1. It consists of a droplet generation device with temperature control, a metal substrate placed in a thermostatic chamber, and a camera. Drop tests were conducted using an industrial paraffin HNP-9 (Nippon Seiro). Material properties of HNP-9 were measured in the previous studies [8 22]. Several selected properties are presented in Table 1. The paraffin was melted in an aluminum holder which was wrapped by a heater. A needle with an inner diameter of 3.0 mm was inserted in the bottom of the holder so that droplets were generated and controlled by turning the micrometer head (MHH2-50, Mitsutoyo). The droplet was detached from the holder when its weight exceeded the surface tension force. The temperature of droplets was measured and controlled by a thermocouple (Type K, 0.32-mm wire diameter) attached to the bottom of the holder. An HNP-9 droplet had a mass of 18.6 $\pm$ 0.6 mg when the droplet temperature was set to 140 °C. During the drop test, the droplet was impacted onto a 430 stainless steel disc substrate with roughness of Rq = 38 nm, diameter of 95 mm, and thickness of 0.5 mm. The surface topology of the substrate was measured by laser microscopy (VK-9700, Keyence) and shown in Fig. 2. The substrate temperature was measured by a thermocouple (Type K, 0.32-mm wire diameter) attached to the center of back surface, and controlled by a thermostatic chamber with a vacuum thermal insulation jacket (BT-100, Sugiyama-Gen). The impact movies were recorded by a digital camera (D3300, Nikon) to observe the debonding behaviors of solidified splats.

Drop tests were conducted with considering the effects of (A) substrate pre-set temperature: 0 °C, 10 °C, 20 °C; (B) drop height: 20 mm, 50 mm, 100 mm, 200 mm; and (C) droplet temperature: 80 °C, 100 °C, 110 °C, 120 °C, 140 °C. Three independent tests were carried out for each test condition, and a total of 180 test results were collected.

The drop impact experiment partly models the deposition of thermal-spray particles, including particle flattening, adhesion, and stress generation. Even though paraffin wax droplet has much lower impact

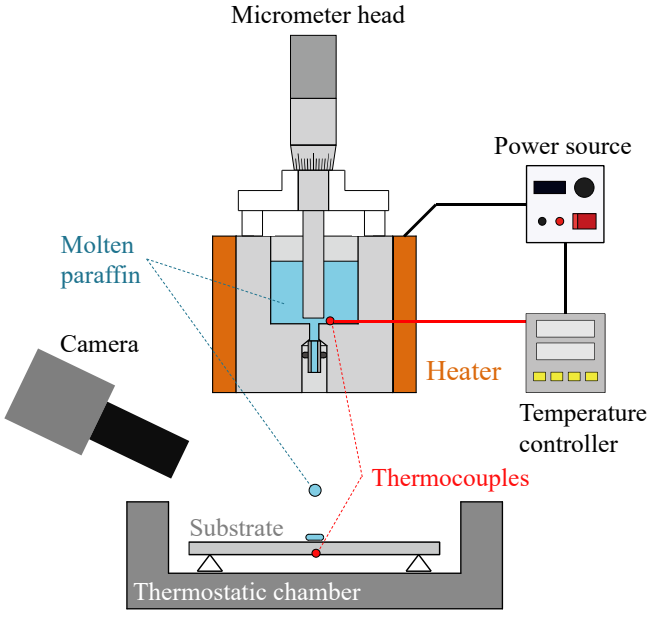

Fig. 1. Schematic illustration of the drop test setup.

Table 1
Material properties of HNP-9 [8 22].

Melting point (°C)	79.8
Young's modulus at 20 °C (GPa)	0.83
Tensile strength at 20 °C (MPa)	2.6
Thermal expansion coefficient (10^{-6}/K)	176
Latent heat of solidification (kJ/kg)	190
Specific heat at 100 °C (kJ/(kg·K))	2.3
Thermal conductivity at 25 °C (W/(m·K))	0.26
Dynamic viscosity at 90 °C (Pa·s)	0.0062
Dynamic viscosity at 140 °C (Pa·s)	0.0030

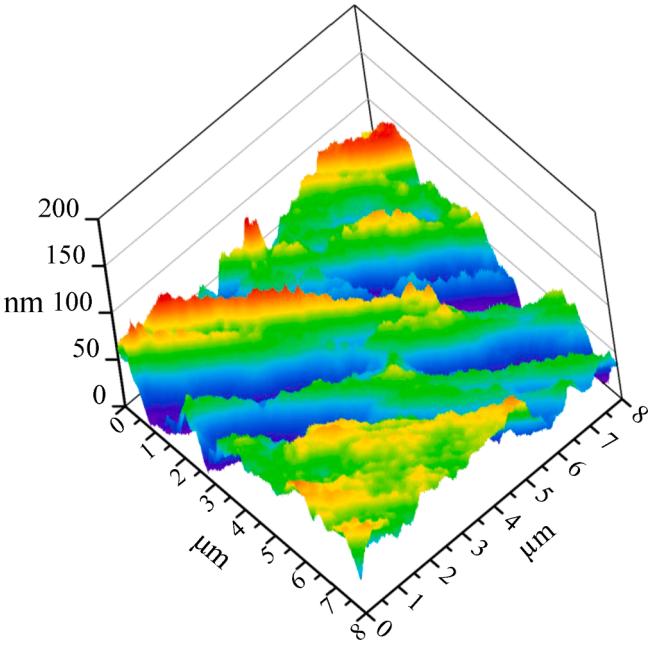

Fig. 2. Surface topology image of 430 stainless steel substrate measured by laser microscopy.

velocity and lower melting point, the mechanisms of adhesion of impacted paraffin wax droplets show high similarity with real thermal spraying particles, that the dominant adhesion mechanisms are both mechanical interlocking, which is highly influenced by droplet characteristics.

Scraping test to measure the interfacial adhesion strength

The scraping test was conducted aiming at evaluating the adhesion strength of solidified splats after the drop test.

Test apparatus

An experimental setup for scraping test is schematically shown in Fig. 3. The stainless steel substrate with a solidified paraffin splat was vertically placed on a steel block. The substrate was completely supported and restricted by a magnet. The width of the cutting blade is 8 mm which is comparable to the splat diameters. The relief angle (α) and rake angle (β) were 6.1° and 54°, respectively. A load cell (DBS-200 N, San-ei Instruments) was installed between the cutting blade and the crosshead of a universal testing machine (LSC-02/30–2, Tokyo Koki Testing Machine). During the scraping tests, the cutting blade was moved vertically downward with a velocity of 10 mm/min until the splat was scraped off completely. The forces in the vertical direction were measured by the load cell during the scraping processes. The blade was slightly pressed onto the substrate so that the splat could be scraped off along the interface. Therefore, a small friction force less than 0.3 N was included in the measured force throughout the scraping processes.

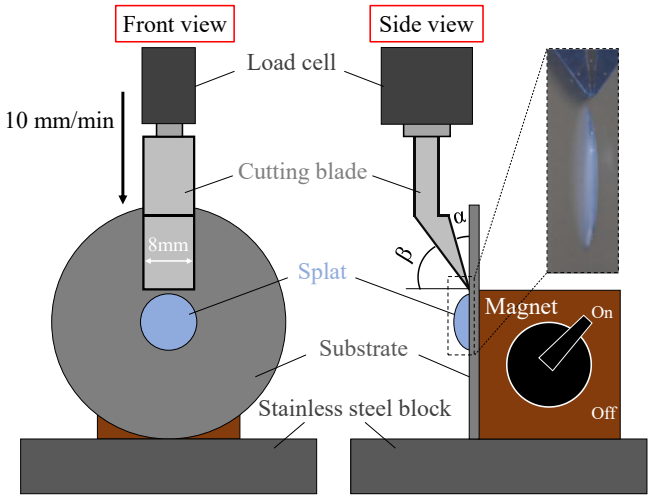

Fig. 3. Schematic illustration of the scraping test setup.

The value of this friction force, which is supposed to be kept constant during the scraping process, was determined by the measured force before the cutting blade starts to scrape off the splat. The scraping force was obtained by subtracting this small friction force from the measured force. The magnet was confirmed not to affect the scraping force.

Test conditions

Scraping tests were conducted under nine test conditions, which are indicated as (1) to (9) in Table 2. The effects of (A) substrate pre-set temperature, (B) drop height (impact velocity), (C) droplet temperature, and (D) residual stress level in splats were examined by six groups of tests as summarized in the table. Groups (D1), (D2) and (D3) were conducted to examine the effect of (D) residual stress for droplet temperatures of 100 °C, 110 °C, and 140 °C, respectively. Three independent tests were conducted for each test condition. All scraping tests were done at an ambient temperature of 20 ± 2 °C.

During the drop tests, residual stresses are generated in splats due to thermal contraction of splats and thermal mismatch between splats and substrates. In the scraping tests, the level of residual stress was changed as a test variable, which was controlled by creep-induced residual stress relaxation. Due to the low melting points of paraffin materials, creep can occur in HNP-9 splats at the ambient temperature of 20 °C [22]. In Table 2, the "Low" residual stress level means that the scraping tests were done when residual stresses in splats were released, which was achieved by placing the substrate with splats for 20 h at ambient temperatures. On the other hand, the "High" residual stress level was achieved by conducting scraping tests immediately after the impact and solidification of droplets. Here, the time interval between the droplet impacts and starting points of scraping tests was unified at 5 min. According to the authors' previous study [22], about 70% of the residual stresses in splats are released after being placed at 20 °C for 20 h, while less than 5% of the stresses are released in the first 5 min. In the drop test, the debonding of splats is influenced by both the adhesion strength and residual stress in splats. To eliminate the effect of the residual stress on scraping test results, as in Table 2, residual stress levels in splats of Groups (A), (B), and (C) were all set to "Low". Scraping tests (7)-(9) were specifically conducted using the splats with high residual stress to examine the effect of (D) residual stress. Detailed information about the stress distribution in high residual stress splats and low residual stress splats will be presented in Sec. 4.2.

Table 2
Conditions of scraping tests.

Conditions of scraping tests	(1)	(2)	(3)	(4)	(5)	(6)	(7)	**(8)**	**(9)**
Substrate pre-set temperature, T_{sub} (°C)	20	10	0	20	20	20	20	20	20
Drop height, H (mm)	50	50	50	50	20	50	50	50	50
Droplet temperature, T_{drop} (°C)	140	140	140	110	140	100	140	110	100
Residual stress level in splats	Low	Low	Low	Low	Low	Low	High	High	High
Groups to examine the effect of each condition									
A: effect of T_{sub}	●	●	●						
B: effect of H	●				●				
C: effect of T_{drop}	●			●		●			
D1: effect of residual stress at T_{drop} = 100 °C						●			●
D2: effect of residual stress at T_{drop} = 110 °C				●				●	
D3: effect of residual stress at T_{drop} = 140 °C	●						●		

Experimental results

Results of drop tests

Fig. 4 summarizes the observed behaviors, in which results of three independent tests are presented for each test condition. Solid circle (●) and triangle (▲) mean debonding and minor debonding, respectively, while hollow circle means (○) no debonding. Debonding was judged according to the photos when the splat temperature was cooled down to the substrate pre-set temperature. The minor debonding was defined as the behavior that debonding area was less than 5% of the interface area. Fig. 5 presents typical photos of solidified splats with (a) debonding, (b) minor debonding, and (c) no debonding. The test condition for each splat is indicated as Fig. 5(a)-(c) in Fig. 4. To clarify the relationship between test conditions and splat debonding, the results in Fig. 4 are replotted in Fig. 6. The symbols in Fig. 6 have the same meaning as those in Fig. 4. In Fig. 6, a "debonding area" is highlighted. The inserts (1)-(9) indicate the nine scraping test conditions as summarized in Table 2.

It is found in Fig. 4 and Fig. 6 that the test conditions significantly affect the debonding behaviors. It can be summarized that the debonding is more likely to occur at lower substrate pre-set temperatures, lower drop heights, and lower droplet temperatures. For a better understanding of the effects of droplet impact conditions on debonding behaviors, geometries of solidified splats were measured by a 3D measuring microscope (VR-3000, Keyence). Typical 3D images of solidified splats with thickness distribution are presented in Fig. 7 when substrate temperatures are (a) 0 °C and (b) 20 °C. Measured profiles along splat diameters are presented in Fig. 8, which reveal the effects of (a) substrate pre-set temperature, (b) drop height, and (c) droplet temperature. These figures reveal that the splat geometry is influenced by the impact conditions; that is thicker splat with a smaller diameter is formed under lower substrate pre-set temperature, lower drop height, and lower droplet temperature.

Results of scraping tests

Displacement-force curves

Generally, two types of test phenomena were observed during the scraping processes. One refers to symmetrical increasing and decreasing of scraping force. The other type of test phenomenon indicates that the splat was completely removed from the substrate associated with the abrupt reduction of scraping force. Typical results for two types of test

● Debonding ▲ Minor debonding ○ No debonding

		T_{sub} : 0 °C			T_{sub} : 10 °C			T_{sub} : 20 °C		
Height	T_{drop}	1st	2nd	3rd	1st	2nd	3rd	1st	2nd	3rd
20 mm	80°C	●	●	●	●	●	●	●	●	●
	100°C	●	●	●	●	●	●	○	○	○
	110°C	●	●	●	●	●	●	○	○	○
	120°C	●	●	●	○	○	●	○	○	○
	140°C	●	●	▲	○	○	○	○	○	○
50 mm	80°C	●	●	●	**Fig. 5(a)** ●	●	●	●	●	●
	100°C	●	●	●	●	●	●	○	○	○
	110°C	●	●	●	**Fig. 5(b)** ▲	▲	▲	○	○	○
	120°C	●	●	●	○	○	○	○	○	○
	140°C	▲	▲	▲	**Fig. 5(c)** ○	○	○	○	○	○
100 mm	80°C	●	●	●	●	●	●	●	●	●
	100°C	●	●	●	○	○	○	○	○	○
	110°C	●	●	●	○	○	○	○	○	○
	120°C	●	●	●	○	○	○	○	○	○
	140°C	○	▲	●	○	○	○	○	○	○
200 mm	80°C	●	●	●	●	●	●	●	●	●
	100°C	●	●	●	○	○	○	○	○	○
	110°C	●	●	●	○	○	○	○	○	○
	120°C	●	●	●	○	○	○	○	○	○
	140°C	○	○	○	○	○	○	○	○	○

Fig. 4. Drop test results. Solid circle means debonding; triangle means minor debonding, in which the debonding area was less than 5% of the interface area; hollow circle means no debonding. Results of three independent tests are presented for each test condition. The inserts of Fig. 5(a)-(c) indicate the test conditions of Fig. 5.

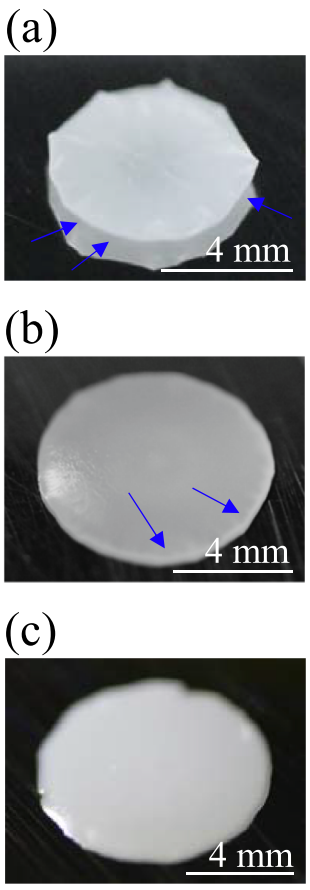

Fig. 5. Typical photos of solidified splats with (a) debonding, (b) minor debonding, and (c) no debonding. Debonding is indicated by blue arrows. The test condition for each splat is indicated as Fig. 5(a)-(c) in Fig. 4. (For interpretation of the references to colour in this figure legend, the reader is referred to the web version of this article.)

phenomena are plotted in Fig. 9 with schematic illustrations of the relevant mechanisms of scraping processes. It is found that three independent tests for each condition show almost comparable displacement-force curves, which confirms that the scraping test in this study reveals well reproducibility. In Fig. 9(a), symmetrical curves are measured due to the symmetrical geometry of the splats. Here, scraping force first increases from the point ① to ③ as the cutting blade moves from the periphery to the center of the splat, where the scraping breadth and splat thickness reach the largest value. The scraping force then decreases with the reduction of scraping breadth and splat thickness until the splat is completely scraped off. Here, the scraping breadth refers to the contacting length between the blade tip and the splat. In Fig. 9(b), the splat is completely removed from the substrate at point ③ associated with rapid reduction of the scraping force. It can be speculated that the removal of splat occurs when the scraping force reaches a critical value inducing rapid crack propagation along the interface.

Measured displacement-force curves under all the nine drop test conditions are presented in Fig. 10 to investigate the effects of (a) substrate pre-set temperature (T_{sub}), (b) drop height (H), (c) droplet temperature (T_{drop}) under low residual stress, and (d) droplet temperature (T_{drop}) under high residual stress. In Fig. 10, only a representative curve is plotted for each test condition. The droplet impact conditions for each scraping test are indicated in Fig. 6 as (1)-(9).

Effects of drop test conditions and residual stress level

The present scraping test provides an interfacial adhesion strength between solidified paraffin splats and metal substrates. It is expected that the measured scraping forces are related to the interfacial adhesion strength, and can be employed to examine the influences of various impact conditions. However, as shown in Fig. 8 the splat geometry changes with droplet impact conditions. It indicates that the measured scraping forces under various conditions cannot be compared directly since the splat geometry intrinsically affects the scraping forces.

To eliminate the effect of splat geometry, Merchant's model of orthogonal cutting is considered [23 24]. In the model, the tangential cutting force can be written as follows:

$$F_c = K_c w h \tag{1}$$

where w is the width of cut and h is the depth of cut. K_c is the tangential cutting force coefficient. Even though K_c might be affected by many factors including depth of cut, a lot of experimental and theoretical studies [25 26 27 28] have suggested that the measured cutting force (F_c) presents an almost linear relationship with depth of cut in orthogonal cutting. Murakawa [19] has examined the effect of coating thickness when evaluating the interfacial adhesion strength using a scraping method. It was found that the measured forces increase almost linearly with the coating thickness even though the adhesion strength is kept constant.

Because the splat geometry (see Fig. 8) and scraping behaviors (see Fig. 9) are affected by the impact conditions, to eliminate these effects, a parameter $K(d)$ is defined to evaluate the adhesion strength as

$$K(d) = \frac{F(d)}{b(d)\cdot t(d)} = \frac{Scraping\,force}{Scraping\,breadth \times Splat\,thickness} \tag{2}$$

Here, $K(d)$ is calculated from the real-time scraping force, $F(d)$, splat thickness, $t(d)$, and scraping breadth, $b(d)$ as a function of scraping displacement d. The scraping breadth $b(d)$ and splat thickness $t(d)$ are determined by splat profiles and displacement-force curves shown in

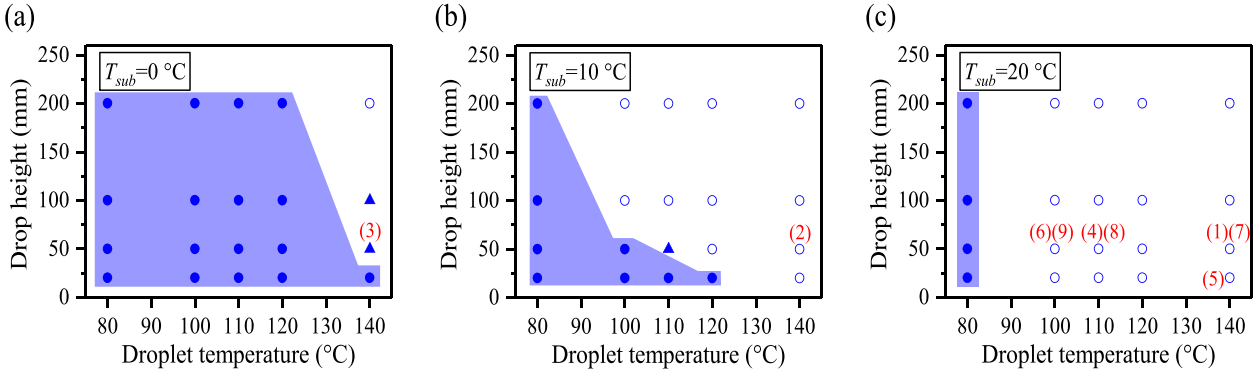

Fig. 6. Drop test results of debonding behaviors when substrate pre-set temperatures (T_{sub}) are (a) 0 °C, (b) 10 °C, and (c) 20 °C. The symbols have the same meaning as those in Fig. 4. A "debonding area" is highlighted. The inserts (1)-(9) indicate the nine scraping test conditions.

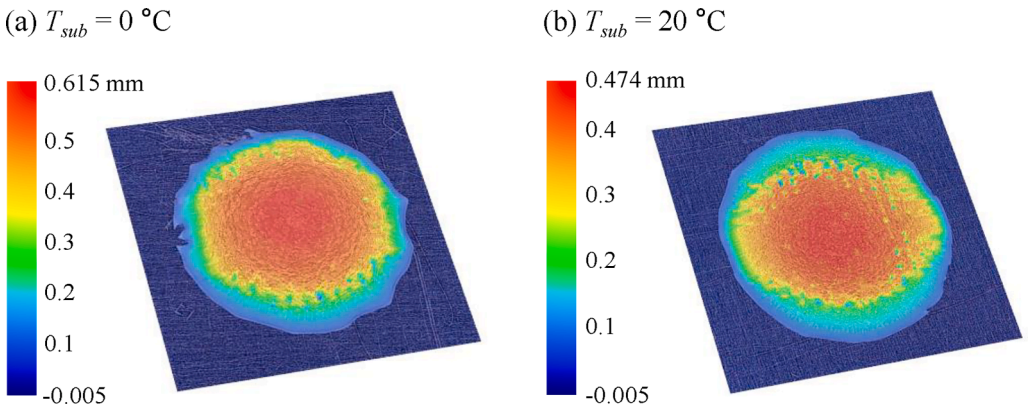

Fig. 7. 3D images of solidified splats with thickness distribution when the substrate temperatures are (a) T_{sub} = 0 °C and (b) T_{sub} = 20 °C. The other impact conditions are same with Fig. 8(a).

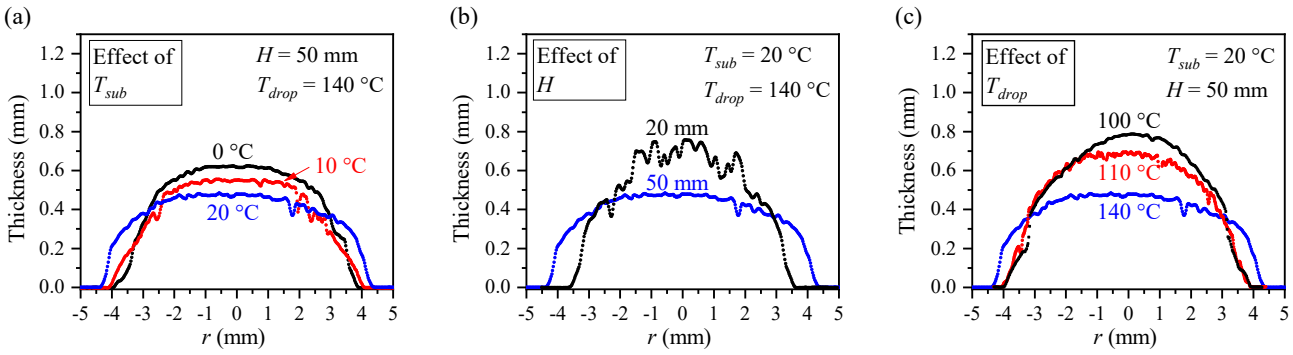

Fig. 8. Measured profiles of solidified splats reveal the effects of (a) substrate pre-set temperature, (b) drop height, and (c) droplet temperature.

Fig. 8 and Fig. 10, respectively. To confirm the reliability of Eq. (2), the calculated $K(d)$ and the measured scraping forces are plotted as a function of scraping displacement in Fig. 11 for scraping tests (1) and (7), which indicate low residual stress condition and high residual stress condition, respectively. In Fig. 11, $K(d)$ for low residual stress condition is always higher than high residual stress condition except for a scraping displacement of 8.5 mm. The values of $K(d)$ are almost constant in the highlighted area when the scraping displacements are between 2 mm and 7 mm. It becomes unstable at the splat peripheries due to the rapid changes in splat thickness, scraping breadth, and scraping force. In this study, the value of $K(d)$ at the maximum scraping force, which is always achieved at a scraping displacement between 2 mm and 7 mm, was defined as K_0 to evaluate the interfacial adhesion strength.

The measured maximum scraping forces (F_{max}) and calculated K_0 are summarized in Fig. 12 to consider the effects of (a) substrate pre-set temperature, (b) drop height, and (c) droplet temperature, where the drop test conditions are identical with those in Fig. 10(a)-(c). It can be seen from Fig. 12(a)-(c) that the maximum scraping forces F_{max} seem not influenced by test conditions. Nevertheless, values of K_0, which eliminates the effect of splat geometry, becomes larger at a higher substrate pre-set temperature, a higher drop height, and a higher droplet temperature. Since larger K_0 corresponds to higher adhesion strength, the scraping test results of K_0 agree well with the debonding behaviors as revealed in Fig. 4 and Fig. 6, where the debonding is prone to occur under those conditions with smaller K_0. The effect of residual stress on K_0 is shown in Fig. 12(d), where the K_0 values for low residual stress and high residual stress conditions are compared. Smaller K_0 values are obtained for high residual stress splats because the high residual tensile stress facilitated the cracking to propagate along the interface and reduced the forces required to scrape off the splats. The experimental results of the drop tests and the scraping tests will be comprehensively discussed in Sec. 4.

Discussions

Effects of impact conditions and residual stress

It is generally accepted that interfacial debonding occurs when the peeling stress and interfacial shear stress exceed the adhesion strength [8]. In thermal spraying, the bonding between coating and substrate is mainly associated with the mechanical interlocking, which is highly related to the roughness of substrate surface and the characteristics of impacting droplets [5 6 29 30]. In some cases, inter-diffusion and chemical reactions may take place near the interface and contribute to the bonding when the substrate is partly melted by the high-temperature droplet [6 30]. In this study, because the droplet temperature is low enough compared with the melting point of substrate, the dominant bonding mechanism is expected to be the mechanical interlocking generated when liquid droplets fill and solidify in the cavities of substrate surface. The adhesion strength, therefore, varies with impact conditions which affect the amount of liquid penetration into substrate surface cavities. On the other hand, the driving forces for debonding, which are the peeling stress and the shear stress, are influenced by many factors such as splat geometry, the residual radial stress in splat (σ_{rr}), and interfacial adhesion. In the authors' previous study [8], in particular, the magnitudes of driving forces have been proven to increase with both splat stress (σ_{rr}) and splat thickness (t). In this section, therefore, the effects of droplet impact conditions on debonding driving forces are discussed by focusing on two factors, namely splat stress (σ_{rr}) and splat thickness (t).

Considering an equi-biaxial plane stress state ($\sigma_{rr} = \sigma_{\theta\theta}$ and $\sigma_{zz} = 0$), and ignoring the creep deformation and stress relaxation at the

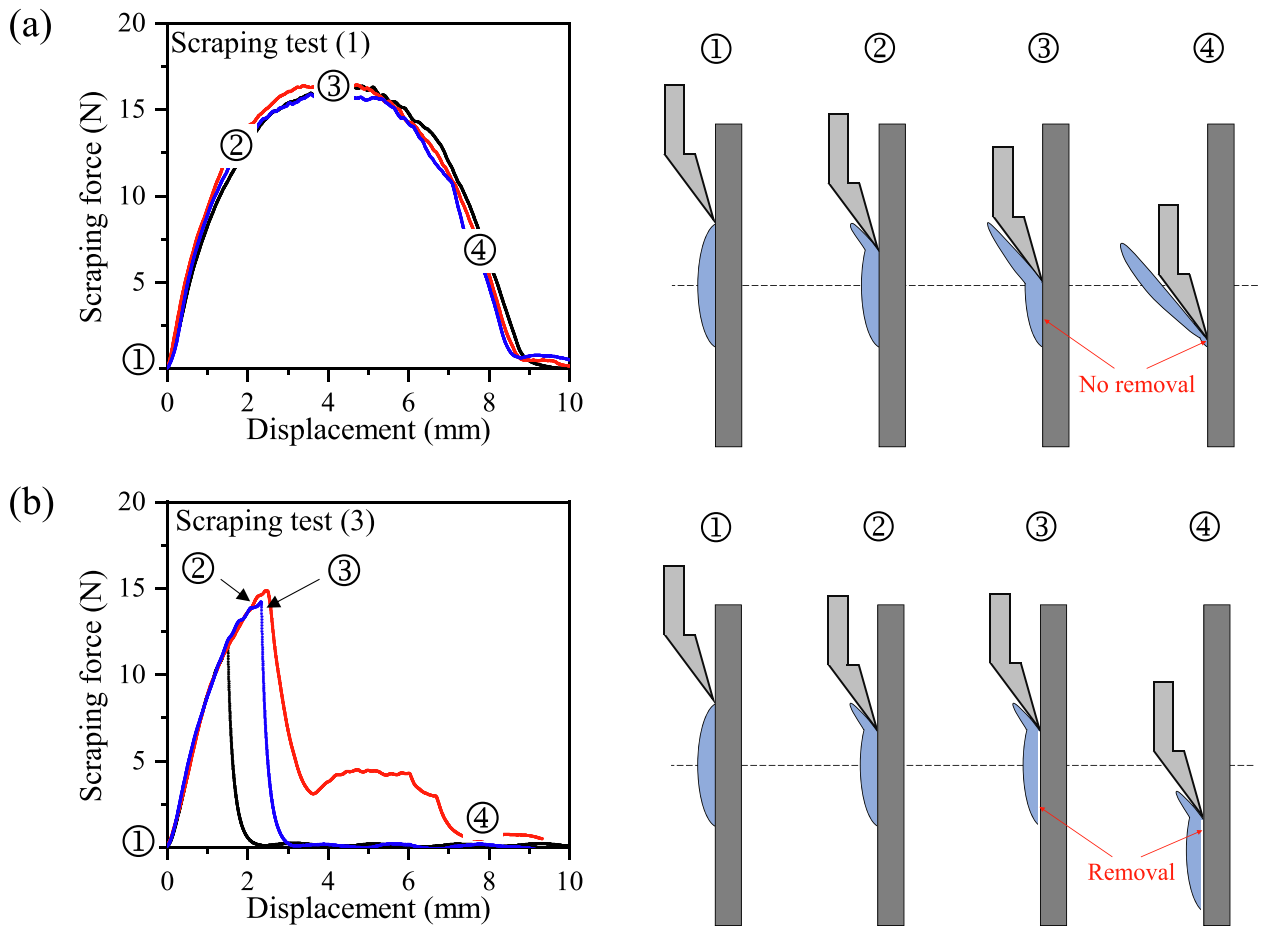

Fig. 9. Typical measurements for two types of test phenomena as well as the schematic illustration of the relevant mechanisms of scraping processes. Three independent tests are conducted for each condition. (a) Scraping test (1), symmetrical increasing and decreasing of scraping force without removal of the splat all through the scraping process. (b) Scraping test (3), abrupt reduction of scraping force when the splat is completely removed.

interface, the splat stress (σ_{rr}) can be described by [8],

$$\sigma_{rr} = \frac{1}{1-\nu} \cdot E_{sp}(T_{sub}) \cdot \alpha_{sp} \cdot (T_{sf} - T_{sub}) \tag{3}$$

where ν, α_{sp}, and T_{sf} refer to Poisson's ratio, thermal expansion coefficient, and stress-free temperature of splat, respectively. T_{sub} refers to substrate pre-set temperature, and E_{sp} (T_{sub}) means Young's modulus of the splat at the temperature of T_{sub}.

Effect of substrate pre-set temperature (T_{sub})

As can be seen in Fig. 4 and Fig. 6, the splats tend to debond during drop tests associated with the reduction of substrate pre-set temperatures. This is caused by the lower interfacial adhesion strength and larger debonding driving forces generated at lower substrate pre-set temperatures. First, the lower substrate pre-set temperatures accelerate the solidification of paraffin droplets, and thereby reduce the amount of liquids that penetrate into the surface cavities of substrates. As a result, the strength of the interfacial mechanical interlocking, which dominates the adhesion strength, becomes lower as substrate temperature decreases. On the other hand, driving forces for debonding increase with the reduction of substrate pre-set temperature due to the larger radial thermal stresses (σ_{rr}) in splats (see Eq. (3)). The larger radial stress generates larger bending moment in substrates, hence inducing larger driving forces at the interface. Additionally, as drawn in Fig. 8(a), the splat thickness (t) becomes larger at lower substrate pre-set temperatures, which can also increase the magnitude of debonding driving forces. The relationship between splat geometries and the magnitude of driving forces will be quantified in Sec. 4.2 using finite element analyses.

Scraping test results of maximum scraping forces and magnitudes of K_0 under various substrate pre-set temperatures are plotted in Fig. 12(a) when the drop height is 50 mm and droplet temperature is 140 °C. It can be seen that the K_0 values monotonically increase with the substrate pre-set temperatures. It explains the phenomenon that splats are more likely to debond at lower substrate pre-set temperatures during the drop tests as discussed in the previous paragraph. At a substrate pre-set temperature of 0 °C, the abrupt reduction of scraping forces is observed as shown in Fig. 10(a). This is caused by a weak interfacial adhesion strength which is overcome by the scraping forces during the scraping processes.

Effect of drop height

As can be seen in Fig. 4 and Fig. 6, debonding is prone to appear at a lower drop height. Similar to the case of substrate pre-set temperature, the effect of drop height on debonding behaviors can be explained by adhesion strength and debonding driving forces. The distribution of the maximum impact pressure of a liquid droplet impacting a solid surface can be described by [31],

$$p(r) = \frac{1}{2}\rho V^2 \cdot e^{-\frac{r^2}{A_2}} \tag{4}$$

where ρ and V are the density and velocity of the splat; r refers to the radial coordinate. A_2 can be written as

$$A_2 = -4R^2 \left[ln \frac{10^{-10}}{\frac{1}{2}\rho V^2} \right]^{-1} \tag{5}$$

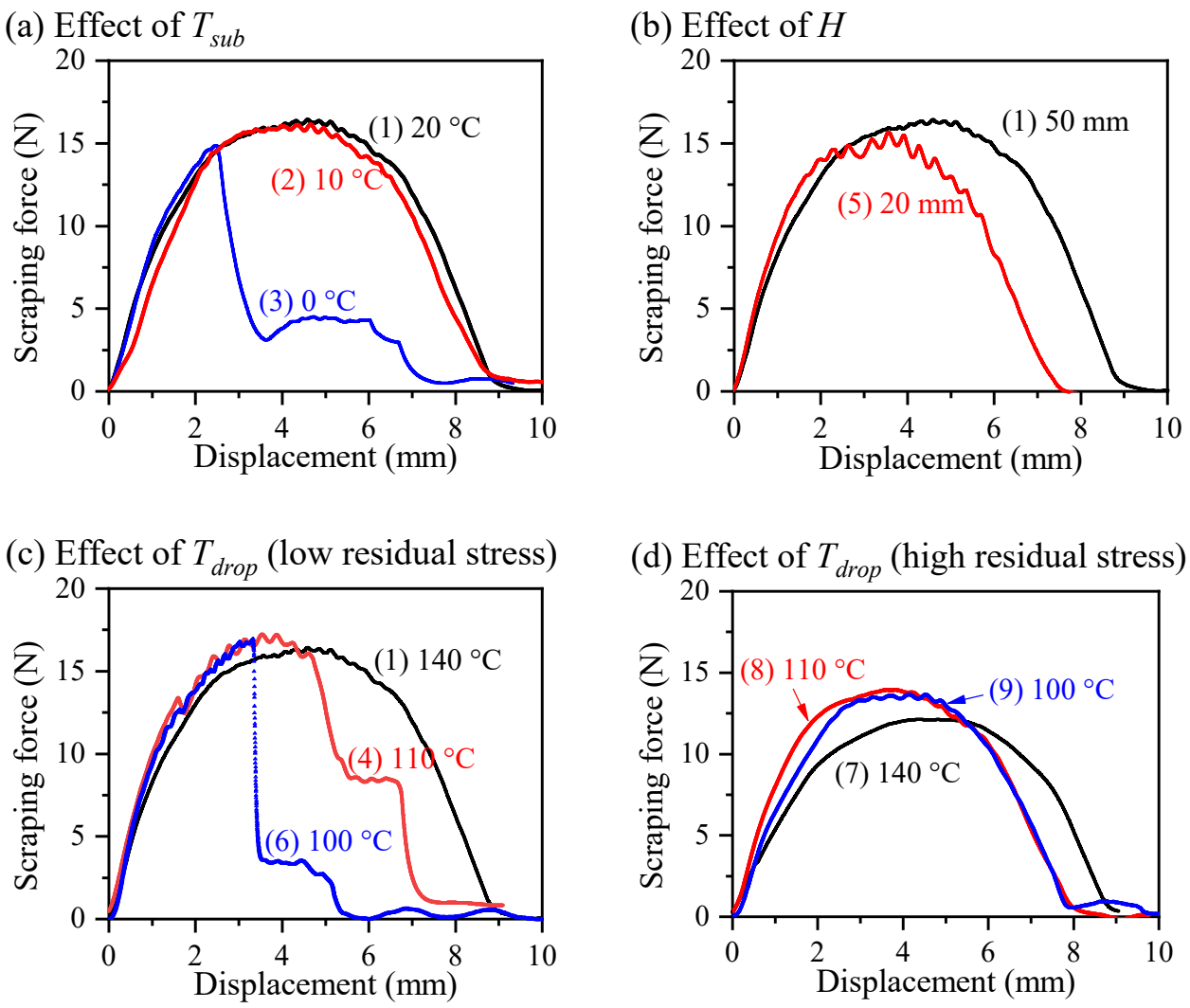

Fig. 10. Measured scraping forces as a function of scraping displacement to investigate the effects of (a) substrate pre-set temperature (T_{drop}), (b) drop height (H), (c) droplet temperature (T_{drop}) under low residual stress, and (d) droplet temperature (T_{drop}) under high residual stress. The droplet impact conditions for each scraping test are indicated in Fig. 6 as (1)-(9).

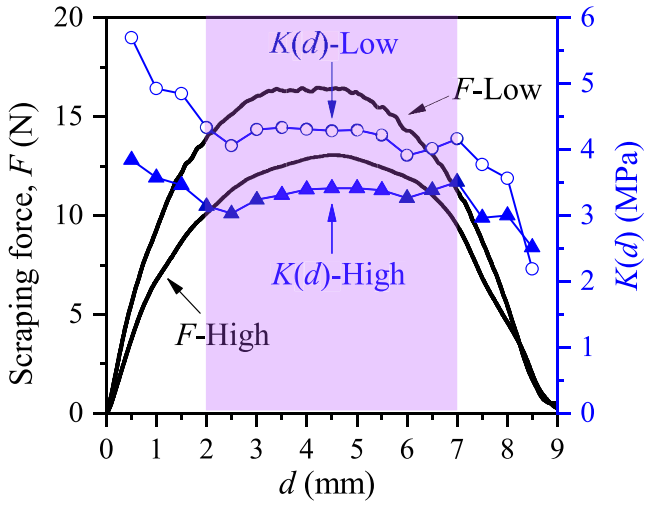

Fig. 11. Calculated $K(d)$ as well as measured scraping forces as a function of scraping displacement under low residual stress condition and high residual stress condition for scraping tests (1) and (7), respectively.

where R is the splat radius. It is found in Eq. (4) and Eq. (5) that pressure, p, becomes larger at a higher drop height which induces higher impact velocity, V. It suggests that larger amount of liquids can be pressed into surface cavities to form a stronger bonding at a higher drop height. On the other hand, driving forces for debonding increase with the reduction of drop height due to the thicker splat (see Fig. 8(b)) associated with the lower impact velocity. Consequently, the larger driving forces coupled with the weaker interfacial adhesion strength caused the splat to debond at a lower drop height.

Maximum scraping forces and values of K_0 are plotted in Fig. 12(b), where the drop heights are 20 mm and 50 mm fixing the substrate pre-set temperature at 20 °C and droplet temperature at 140 °C. The values of K_0 are larger for drop height of 50 mm owing to the higher impact velocity to form stronger interfacial adhesion, which is in good accordance with the results of drop tests.

Effect of droplet temperature (T_{drop})

Droplet temperature is another important factor that influences debonding behaviors. Lower droplet temperatures facilitate the occurrence of debonding as seen in Fig. 4 and Fig. 6. This can be explained by the weaker interfacial adhesion and larger debonding driving forces generated at lower droplet temperatures. First, owing to low droplet temperatures, the adhesion strength becomes weak due to the quick

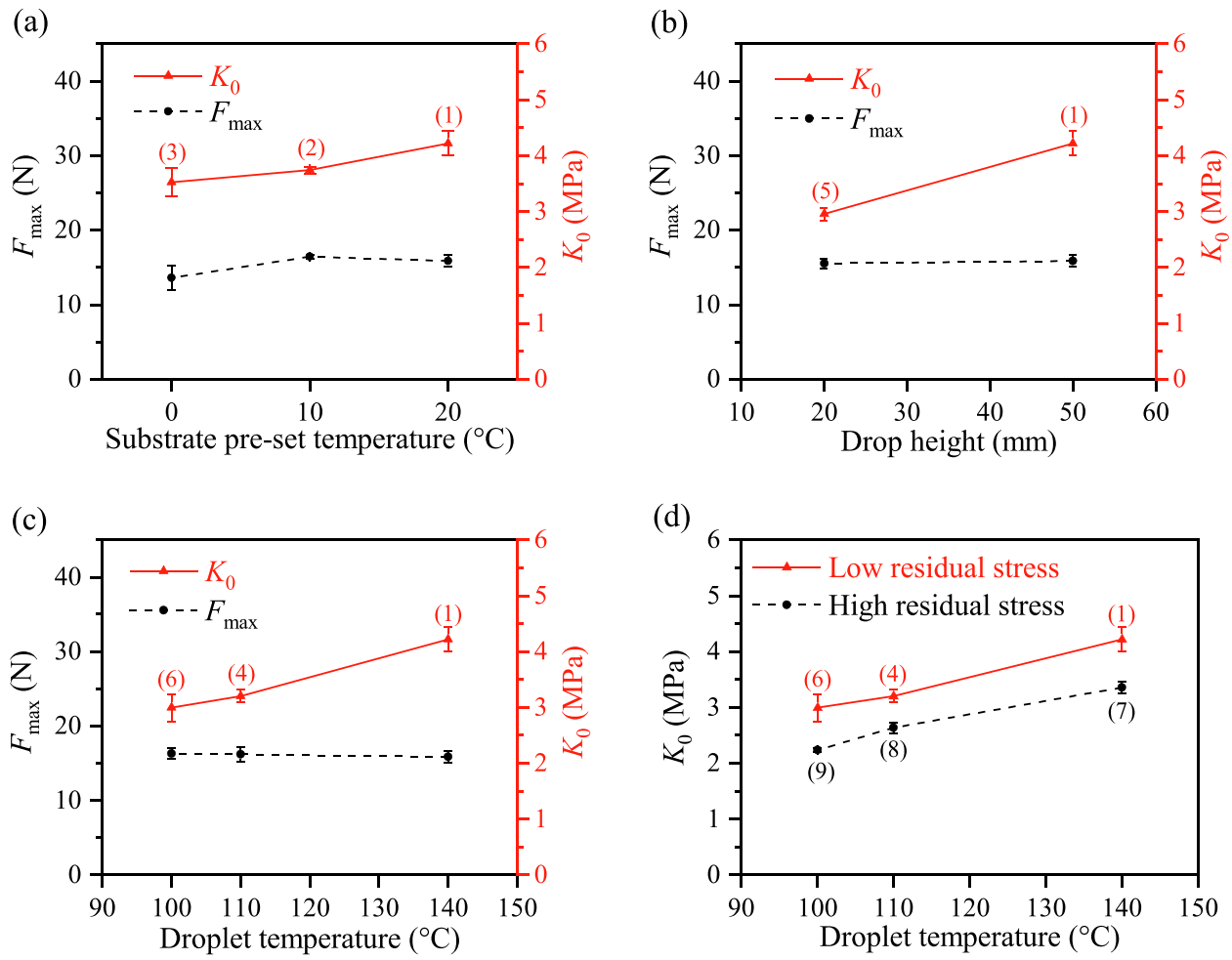

Fig. 12. Summary of the maximum scraping forces (F_{max}) and calculated K_0. The effects of (a) substrate pre-set temperature, (b) drop height, and (c) droplet temperature on F_{max} and K_0 are presented. And the effects of (d) droplet temperature and residual stress on K_0 are also shown.

solidification process and also due to the larger viscosities which prevent the liquid from flowing into substrate cavities. Second, the splats formed under lower droplet temperatures are thicker (see Fig. 8(c)) due to larger viscosities which restrict the droplets to spread. As discussed above, the thicker splats always generate larger driving forces for debonding.

Fig. 12(c) presents the effect of droplet temperatures on the maximum scraping forces and K_0 values when substrate pre-set temperature is 20 °C and drop height is 50 mm. The K_0 values increase with droplet temperatures. It can be found in Fig. 10(c) that the removal of splats occurs earlier as the droplet temperature decreases. It agrees well with drop test results, where the lower droplet temperatures facilitated debonding of splats.

In summary, by investigating the K_0 values under various drop test conditions, the results of scraping tests showed good agreement with debonding behaviors observed in the drop tests. That is, the smaller K_0 values were obtained for the conditions when debonding occurred more easily.

Effect of residual stress

Accurate investigation for the effect of residual stress on interfacial adhesion strength of thermally sprayed coatings has been a tough work because the change of residual stress is always associated with the simultaneous changes in many other factors such as coating thickness, Young's modulus, and porosity. In this scraping test, the residual stress in splats can be independently controlled by the stress relaxation of splats without any changes in other factors. The residual stress, therefore, is the only variable to affect the interfacial adhesion strength. Detailed comparison of stress distribution under low and high residual stress conditions will be numerically calculated and presented in Sec. 4.2.

The measured scraping forces under low and high residual stresses are plotted in Fig. 10(c) and (d), respectively for various droplet temperatures, fixing the substrate pre-set temperature at 20 °C and drop height at 50 mm. At a droplet temperature of 140 °C, the removal of splats does not occur in either high residual stress or low residual stress condition. The maximum value and increasing rate of scraping forces for low residual stress condition are higher than those for high residual stress condition. This is because the high residual tensile stress facilitates the cracking along the interface. Test results for 110 °C show that the removal of splat occurs in the low residual stress condition. The removal, however, does not appear for high residual stress condition because the higher residual tensile stress reduces the magnitude of scraping forces so that it does not reach the critical values to remove the splats from the substrate. As shown in Fig. 10(c), when droplet temperature reduces from 110 °C to 100 °C, the removal of splats occurs at smaller displacements. This is caused by the weaker interfacial adhesion at lower droplet temperatures.

Fig. 12(d) compares the calculated K_0 for high and low residual stress conditions under various droplet temperatures. The K_0 values for low residual stress condition are always larger than high residual stress

condition. As has been discussed above, this result is caused by the residual tensile stress which slows down the increasing rate of scraping forces. Quantification for the effect of residual stress on interfacial adhesion strength is a rather difficult task because of the complex mechanisms of fracture behaviors and stress generation/relaxation processes during the scraping tests. Further study is required towards a better and in-depth understanding of the relationship between residual stress level and interfacial adhesion strength.

Finite element simulation

Finite element model and simulation conditions

Finite element (FE) simulation is conducted to calculate the stresses which are generated in solidified splats due to thermal contraction and thermal mismatch between splats and substrates. Two types of simulations are conducted using the commercial finite element code ABAQUS/Standard 2017. One is an elastic-creep analysis aiming to compare the stress distributions under high and low residual stress conditions. The other is a coupled thermo-mechanical analysis for evaluating the debonding behaviors via computing the interfacial stresses under various droplet impact conditions.

Axisymmetric FE models are built where the dimensions of splats and substrates are determined according to the actual drop tests. An example of the axisymmetric FE model is presented in Fig. 13, where the model geometry is simulating the actual shape when the substrate pre-set temperature is 20 °C; drop height is 50 mm; and droplet temperature is 140 °C. Fine mesh with the smallest size of 10 μm is distributed near the interface. The geometries of splats are simplified as trapezoids based on the measured profiles as shown in Fig. 8. Detailed descriptions of all the material properties can be found in the previous publication [22].

The stress distribution under high/low residual stress condition is calculated by an elastic-creep analysis, in which an elastic simulation is first conducted to reproduce the actual stress state in the splats based on the measured quenching strains at substrate back surface. A subsequent creep analysis is employed to simulate the residual stress depending on holding time. In this study, a low residual stress condition of HNP-9 splats refers to a holding time of 20 h, while a high residual stress condition is achieved under a holding time of 5 min. The shear stress (τ_{rz}) along the interface and the peeling stress (σ_{zz}) normal to the interface, are recognized as the driving forces for debonding during drop tests. They are calculated by using a coupled thermo-mechanical analysis for the drop test conditions identical to those of Fig. 8(b) and (c) to investigate the effects of drop heights: 20 mm, 50 mm, and droplet temperatures: 100 °C, 110 °C, and 140 °C. In the coupled thermo-mechanical analysis, the stress variation associated with thermal conduction between splats and substrates is computed.

Simulation results of elastic-creep analysis

Residual stress distributions at the interface along the radial direction (σ_{rr}) are compared in Fig. 14(a) for high residual stress and low residual stress conditions. It can be seen that σ_{rr} decreases from 1.5 MPa to 0.5 MPa when the holding time increases from 5 min to 20 h. Calculated peeling stresses (σ_{zz}) and shear stresses (τ_{rz}) distributions along the interface are plotted in Fig. 14(b) and (c), respectively. Similar to σ_{rr}, interfacial stresses are significantly released with a holding time of 20 h.

It is also found that splat stress σ_{rr} keeps constant along the radial direction. The peeling stress σ_{zz} is tensile near the free edge and changes to compressive at $r \approx 3$ mm. This compressive stress, which becomes maximum at $r \approx 2$ mm, is due to the bending moment induced by the thermal shrinkage of the splat. The shear stress along the interface τ_{rz} shows the maximum value at the free edge and decreases towards the center of the model. The driving forces for debonding are shear stress τ_{rz} and tensile peeling stress σ_{zz}. They all reach the maximum value at the periphery of the splat. This result agrees well with the experimental phenomenon that debonding always initiates from splat periphery.

Simulation results of coupled thermo-mechanical analysis

Calculated results for several test conditions are presented in Fig. 15 and Fig. 16 where peeling stresses and shear stresses along the interface are plotted. During the drop tests, debonding always initiated from the periphery of splats. In this section, therefore, the stresses at the splat edges will be focused to evaluate the effects of drop heights (Fig. 15) and droplet temperatures (Fig. 16) on the driving forces for debonding during the drop tests. Here, the ranges of r for every curve in the figures are different due to the different splat diameters formed.

Fig. 15 compares the stress distributions for drop heights of 20 mm and 50 mm, where Fig. 15(a) and (b) show peeling stress and shear stress, respectively. The magnitudes of both peeling and shear stresses at the splat edges are larger in the drop height of 20 mm. It is owing to the thicker splat (see Fig. 8(b)) formed at the lower drop height, which induces larger bending moment and larger stresses at the interface as discussed in Sec. 4.1. The calculation results show good agreement with the results of drop test in which the debonding is more likely to occur at lower drop heights.

Fig. 16 summarizes the calculation results for three various droplet temperatures: 100 °C, 110 °C, and 140 °C, fixing the substrate pre-set temperature at 20 °C and drop height of 50 mm. It can be seen that

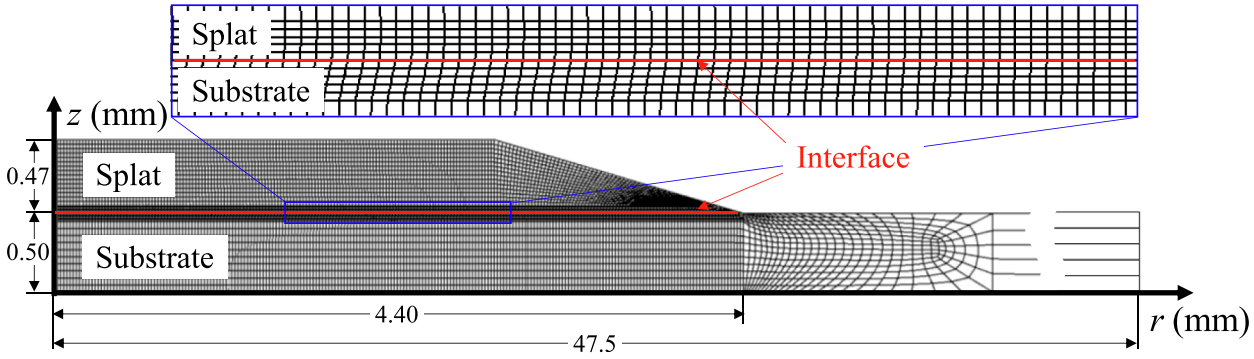

Fig. 13. An example of the axisymmetric finite element model when the substrate pre-set temperature is 20 °C; drop height is 50 mm; and droplet temperature is 140 °C. Fine mesh with the smallest size of 10 μm is distributed near the interface.

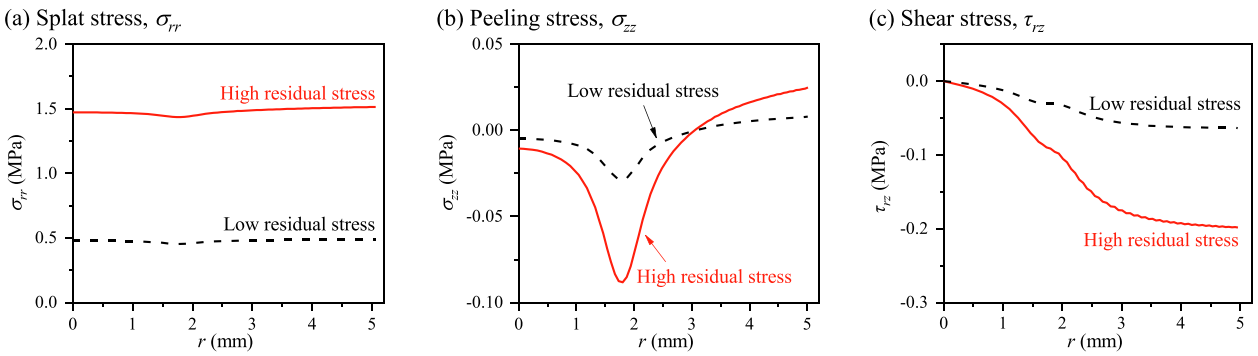

Fig. 14. Numerical results of residual stress distributions at the interface along the radial direction: (a) splat stress (σ_{rr}), (b) peeling stress (σ_{zz}), and (c) shear stress (τ_{rz}) for low residual stress condition and high residual stress condition.

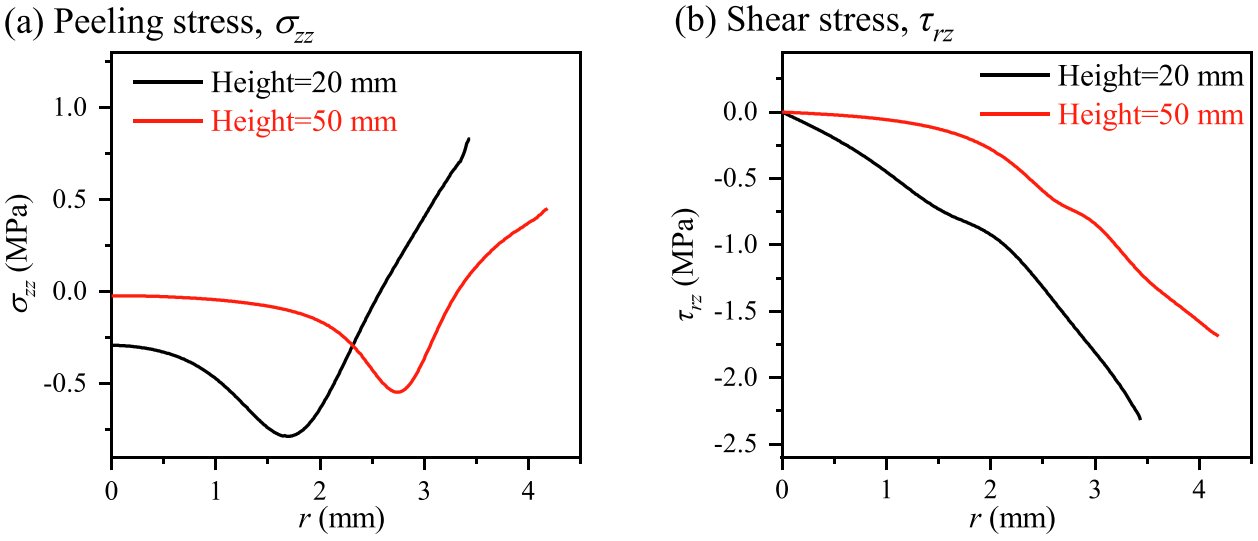

Fig. 15. FEM results of (a) peeling stress and (b) shear stress distributions at the interface along the radial direction when drop heights are 20 mm and 50 mm, fixing the substrate pre-set temperature at 20 °C and droplet temperature at 140 °C.

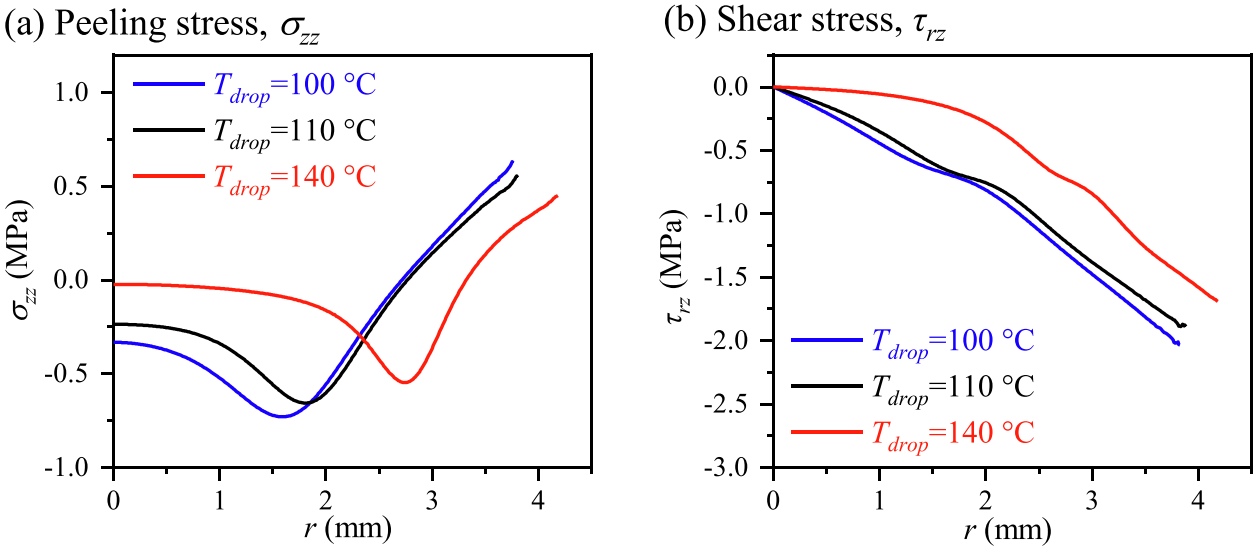

Fig. 16. FEM results of (a) peeling stress and (b) shear stress distributions at the interface along the radial direction when droplet temperatures are 100 °C, 110 °C, and 140 °C, fixing the substrate pre-set temperature at 20 °C and drop height of 50 mm.

both peeling stresses and shear stresses at splat edges increase with reducing droplet temperatures. It is owing to the higher viscosities of droplets at lower droplet temperatures which causes thicker splats, thereby generating larger interfacial stresses. The calculation results agree well with drop test results where the debonding is prone to occur at lower droplet temperatures.

Conclusions

Debonding behaviors of paraffin droplet impacted and solidified on a stainless steel substrate were experimentally observed, considering the effects of substrate pre-set temperature, drop height, and droplet temperature. The splat-substrate adhesion strength was then measured by using a scraping method with consideration of the effects of drop test conditions and residual stress. The driving forces for debonding during the drop tests were evaluated through a coupled thermo-mechanical FE analysis. The results of scraping tests and FE simulations provided reasonable explanations for the debonding behaviors observed during the drop tests. The main results are summarized as follows.

- Paraffin drop test provides experimental and numerical evidence promoting an understanding of the effects of drop impact conditions on interfacial adhesion strength and interfacial debonding driving forces.
- Debonding was more likely to occur at lower substrate pre-set temperatures, lower drop heights, and lower droplet temperatures. This is governed by both the interfacial adhesion strength and the values of driving forces.
- In the scraping test, a parameter, K_0 which eliminates the effect of splat geometry was defined to evaluate the adhesion strength. Smaller K_0 values were measured at lower substrate pre-set temperatures, lower drop heights, and lower droplet temperatures. These tendencies successfully explain the debonding behaviors observed in the drop impact test.
- The level of residual tensile stresses in splats was controlled by stress relaxation treatment to examine its effect on the adhesion strength. The scraping test results suggested that the residual stresses facilitated the cracking to propagate along the interface, thereby reducing the measured scraping forces.
- The effect of the stress relaxation treatment on the residual stresses was verified by FE analysis. In addition, FE analysis indicated that larger driving forces (peeling stresses and shear stresses) are generated at lower drop heights and lower droplet temperatures. It explains the debonding behavior observed in the drop impact test well.

This study employs a scraping method to study the adhesion strength of single splats, in which the effect of drop impact conditions can be evaluated. The results give insight into the optimization of thermal spraying, that particle impact conditions significantly affect the interfacial mechanical interlocking, and hence interfacial adhesion strength and interfacial debonding behaviors. It is, therefore, of great importance to find appropriate particle impact conditions for achieving high interfacial bonding strength.

CRediT authorship contribution statement

Chao Kang: Conceptualization, Methodology, Writing – original draft, Software. **Motoki Sakaguchi:** Investigation, Writing – review & editing, Supervision, Project administration, Funding acquisition. **Akito Saito:** Methodology. **Hirotsugu Inoue:** Supervision, Writing – review & editing.

Declaration of Competing Interest

The authors declare that they have no known competing financial interests or personal relationships that could have appeared to influence the work reported in this paper.

Acknowledgments

This study was supported by JSPS KAKENHI Grant-in-Aid for Scientific Research (B) 21H01206. Chao Kang would like to acknowledge the financial support from China Scholarship Council (CSC).

References

[1] Rhys-Jones TN. The use of thermally sprayed coatings for compressor and turbine applications in aero engines. Surf Coat Technol 1990;42(1):1–11. https://doi.org/10.1016/0257-8972(90)90109-P.
[2] Gérard B. Application of thermal spraying in the automobile industry. Surf Coat Technol 2006;201(5):2028–31. https://doi.org/10.1016/j.surfcoat.2006.04.050.
[3] Schneider KE, Belashchenko V, Dratwinski M, Siegmann S, Zagorski A, editors. Thermal Spraying for Power Generation Components. John Wiley & Sons Wiley; 2006.
[4] Fauchais P, Vardelle A, Dussoubs B. Quo Vadis Thermal Spraying ? J Therm Spray Technol 2001;10(1):44–66. https://doi.org/10.1361/105996301770349510.
[5] Lima CRC, Guilemany JM. Adhesion improvements of Thermal Barrier Coatings with HVOF thermally sprayed bond coats. Surf Coat Technol 2007;201(8):4694–701. https://doi.org/10.1016/j.surfcoat.2006.10.005.
[6] Sobolev VV, Guilemany JM, Nutting J, Miquel JR. Development of substrate-coating adhesion in thermal spraying. Int Mater Rev 1997;42(3):117–36. https://doi.org/10.1179/imr.1997.42.3.117.
[7] Matejicek J, Sampath S. Intrinsic residual stresses in single splats produced by thermal spray processes. Acta Mater 2001;49(11):1993–9. https://doi.org/10.1016/S1359-6454(01)00099-4.
[8] Kang C, Sakaguchi M, Amano A, Kurokawa Y, Inoue H. Quenching stress and fracture of paraffin droplet during solidification and adhesion on metallic substrate. Surf Coat Technol 2019;374:868–77. https://doi.org/10.1016/j.surfcoat.2019.06.067.
[9] Staia MH, Ramos E, Carrasquero A, Roman A, Lesage J, Chicot D, et al. Effect of substrate roughness induced by grit blasting upon adhesion of WC-17% Co thermal sprayed coatings. Thin Solid Films 2000;377-378:657–64. https://doi.org/10.1016/S0040-6090(00)01447-4.
[10] Okajima Y, Sakaguchi M, Inoue H. A finite element assessment of influential factors in evaluating interfacial fracture toughness of thermal barrier coating. Surf Coat Technol 2017;313:184–90. https://doi.org/10.1016/j.surfcoat.2017.01.052.
[11] Zhou F, Zhang Z, Liu S, Wang L, Jia J, Wang Y, et al. Effect of heat treatment and synergistic rare-earth modified NiCrAlY on bonding strength of nanostructured 8YSZ coatings. Appl Surf Sci 2019;480:636–45. https://doi.org/10.1016/j.apsusc.2019.02.247.
[12] ASTM, D4541, Standard test method for pull-off strength of coatings using portable adhesion testers; 2017.
[13] ASTM, C633-01, Standard test method for adhesion or cohesion strength of thermal spray coatings; 2017.
[14] Balić EE, Hadad M, Bandyopadhyay PP, Michler J. Fundamentals of adhesion of thermal spray coatings: Adhesion of single splats. Acta Mater 2009;57(19):5921–6. https://doi.org/10.1016/j.actamat.2009.08.042.
[15] Goldbaum D, Shockley JM, Chromik RR, Rezaeian A, Yue S, Legoux J-G, et al. The effect of deposition conditions on adhesion strength of Ti and Ti6Al4V cold spray splats. J Therm Spray Technol 2012;21(2):288–303. https://doi.org/10.1007/s11666-011-9720-3.
[16] Chen SY, Ma GZ, Wang HD, He PF, Wang HM, Liu M. Evaluation of adhesion strength between amorphous splat and substrate by micro scratch method. Surf Coat Technol 2018;344:43–51. https://doi.org/10.1016/j.surfcoat.2018.02.073.
[17] Dickinson ME, Yamada M. A New Method for Measuring Shear Adhesion Strength of Ceramic Cold Spray Splats. Nanosci Nanotechnol Lett 2010;2(4):348–51. https://doi.org/10.1166/nnl.2010.1106.
[18] Kar S, Bandyopadhyay PP. Scratch induced damage in alumina splats deposited on bond coats. J Mater Process Technol 2011;211(4):553–9. https://doi.org/10.1016/j.jmatprotec.2010.10.021.
[19] Murakawa M, Takeuchi S. Quantitative adhesion strength measurement of diamond coatings. Thin Solid Films 1989;181(1-2):443–50. https://doi.org/10.1016/0040-6090(89)90513-0.
[20] Xie Z, Zhu J, Guo W. The scraping test and adhesion measurements of diamond and nickel electroless coatings. Mater Charact 2000;44(4-5):347–52. https://doi.org/10.1016/S1044-5803(00)00063-2.
[21] Amano A, Sakaguchi M, Kurokawa Y, Okajima Y, Inoue H. Measurement of quenching strain in paraffin drop test modelling thermal spray process. Trans JSME 2017;83:1–14. https://doi.org/10.1299/transjsme.17-00377 (in Japanese).

[22] Kang C, Sakaguchi M, Inoue H. Contribution of creep to strain evolution in a paraffin droplet during and after rapid solidification on a metal substrate. Surf Coat Technol 2020;399:126145. https://doi.org/10.1016/j.surfcoat.2020.126145.
[23] Merchant ME. Mechanics of the metal cutting process. I. Orthogonal cutting and a type 2 chip. J Appl Phys 1945;16(5):267–75. https://doi.org/10.1063/1.1707586.
[24] Stephenson DA, Agapiou JS. Metal cutting theory and practice. 3rd edition,. CRC Press; 2016. p. 418.
[25] Nishimatsu Y. The mechanics of rock cutting. Int J Rock Mech Min Sci 1972;9(2):261–70. https://doi.org/10.1016/0148-9062(72)90027-7.
[26] Chinchanikar S, Choudhury SK. Effect of work material hardness and cutting parameters on performance of coated carbide tool when turning hardened steel: An optimization approach. Measurement 2013;46(4):1572–84. https://doi.org/10.1016/j.measurement.2012.11.032.
[27] Jadhav JS, Jadhav BR. Experimental Study of Effect of Cutting Parameters on Cutting Force in Turning Process. Int J Innov Res Adv Eng. 2014;1:240–8.
[28] Kumar A, Mahapatra MM, Jha PK. Effect of machining parameters on cutting force and surface roughness of in situ Al–4.5%Cu/TiC metal matrix composites. Measurement 2014;48:325–32. https://doi.org/10.1016/j.measurement.2013.11.026.
[29] Mohammadi Z, Ziaei-Moayyed AA, Mesgar A-M. Grit blasting of Ti–6Al–4V alloy: Optimization and its effect on adhesion strength of plasma-sprayed hydroxyapatite coatings. J Mater Process Technol 2007;194(1-3):15–23. https://doi.org/10.1016/j.jmatprotec.2007.03.119.
[30] Fauchais P, Fukumoto M, Vardelle A, Vardelle M. Knowledge concerning splat formation: an invited review. J Therm Spray Technol 2004;13(3):337–60. https://doi.org/10.1361/10599630419670.
[31] Xue M, Chandra S, Mostaghimi J, Salimijazi HR. Formation of pores in thermal spray coatings due to incomplete filling of crevices in patterned surfaces. Plasma Chem Plasma Process 2007;27(5):647–57. https://doi.org/10.1007/s11090-007-9097-8.